

Ideal strength of ferromagnetic Fe-based alloys from first-principles theory

Xiaoqing Li,^{1,*} Stephan Schönecker,^{1,†} Jijun Zhao,^{2,3,‡} Börje Johansson,^{1,4} and Levente Vitos^{1,4,5}

¹*Applied Materials Physics, Department of Materials Science and Engineering,
Royal Institute of Technology, Stockholm SE-10044, Sweden*

²*School of Physics and Optoelectronic Technology and College of Advanced Science and Technology,
Dalian University of Technology, Dalian 116024, China*

³*Key Laboratory of Materials Modification by Laser,
Electron, and Ion Beams (Dalian University of Technology),
Ministry of Education, Dalian 116024, People's Republic of China*

⁴*Department of Physics and Astronomy, Division of Materials Theory,
Uppsala University, Box 516, SE-75120, Uppsala, Sweden*

⁵*Research Institute for Solid State Physics and Optics,
Wigner Research Center for Physics, Budapest H-1525, P.O. Box 49, Hungary*

(Dated: April 19, 2013)

The all-electron exact muffin-tin orbitals method in combination with the coherent-potential approximation has been employed to investigate the ideal tensile strengths of bcc ferromagnetic Fe and $\text{Fe}_{1-x}\text{M}_x$ ($M=\text{Cr, Ni, Al, Co, Mn, and V}$) random alloys in the [001] direction. The present ideal strength is calculated to be 11.0 GPa for pure bcc Fe, in good agreement with the available theoretical data. For the Fe-based alloys, we predict that Co, Cr and V increase the ideal tensile strength, while Ni and Al decrease it. Manganese yields a non-monotonous alloying behavior. We show that the limited use of the previously established ideal tensile strengths model based on structural energy differences in the case of Fe-based alloys is attributed to the effect of magnetism.

I. INTRODUCTION

The mechanical strength of real materials is usually controlled by the occurrence of grain boundaries, cracks, dislocations and other micro-structural defects. If such defects were not present, the strength would be limited by the stress at which the lattice itself becomes unstable with respect to a homogeneous strain. This stress referred to as the ideal strength or ideal tensile strength (ITS) is an upper bound strength of an ideal single crystal. The ideal strength is an inherent property of a defect-free material and can offer insight into the correlation between the intrinsic chemical bonding and the crystal symmetry, and has been accepted as an essential mechanical parameter of single crystal materials.¹ The experimental data on the ideal strength are rather limited. The few available values were obtained from tensile tests for whiskers^{2,3} and from nanoindentation experiments.⁴

In recent years, considerable attention was paid to the computation of the ITS of elements or ordered alloys by first-principle methods. The ideal strength of refractory metals (such as Mo, Nb, V, and W), noble transition metals (such as Cu, Pt and Au), elements crystallizing in the diamond structure (Si, Ge, and C) as well as few ordered alloys (TiAl and Ni_3Al) was extensively investigated.^{5–17} Among the body-centered cubic (bcc) metals, Fe received a great scientific interest.^{1,17–21} It was reported that, the [001] direction of Fe is the weakest direction in response to an uniaxial stress. It has been shown, that a bifurcation from the primary tetragonal deformation path (the Bain path) to a secondary orthorhombic deformation path occurs after the ITS on the primary path is reached.¹ Thus, bcc Fe strained along the [001] direction fails by cleavage and not by shear as opposed to

bcc V and Nb.¹² In spite of all these theoretical efforts, the first-principles description of the ITS in substitutionally disordered alloys is rather limited. Li *et al.*²² investigated the composition dependent ITS of bcc vanadium-based nonmagnetic (NM) random solid solutions alloyed with chromium and titanium in various crystallographic directions employing the coherent potential approximation (CPA). To the best of our knowledge, no experimental or theoretical study has focused on the alloying effect on the ITS of Fe-based alloys. It is the purpose of this paper to bring forward a comprehensive study of the ideal strength to bcc ferromagnetic (FM) Fe-based random alloys.

Iron alloys are the most widely used engineering materials due to their excellent mechanical properties. For example ferritic Fe-Cr-based stainless steels have been considered as the primary structural materials in the first wall and blanket structure of future fusion reactor.^{23,24} Alloying plays a central role in designing advanced engineering materials with desired properties. Different solute atoms produce different effects on fundamental mechanical properties. Previous works focused on the effects of various typical solute atoms on the mechanical properties of Fe in the small deformation region, where the stress-strain relations are linear.^{25–30} However, the ideal strength describes the mechanical properties of the material beyond the elastic region.

In this work, using the exact muffin-tin orbitals method, we study the composition dependence of the ITS of FM $\text{Fe}_{1-x}\text{M}_x$ alloys for various alloying elements, $M=\text{Cr, Ni, Al, Co, Mn, and V}$. The primary purpose of our work is to give an account of the application of the alloy theory to the ITS of bcc FM random alloys. Second, we aim to provide a consistent theoretical guide

to further optimization of the composition of Fe-based alloys in multiscale materials design.

The structure of the manuscript is as follows. In Section II, we describe the computation tool and the important numerical details. The results are presented and discussed in Section III. Here, first we assess the accuracy of our calculations by considering pure bcc Fe. Then we study the effects of the alloying elements on the ideal strength of Fe-based alloys.

II. COMPUTATIONAL METHOD

A. Total energy calculation

The first-principle method used in this work is based on density functional theory (DFT).³¹ We adopted the generalized gradient approximation (GGA) of the Perdew-Burke-Ernzerhof (PBE)³² functional to describe the exchange-correlation interaction, which is well known to give the correct FM bcc ground state for Fe. The Kohn-Sham equations were solved using the EMT0 method.^{33–35} The problem of disorder was treated within the CPA and the total energy is computed via the full charge-density technique.^{36–39}

The EMT0 method is an improved screened Korringa-Kohn-Rostoker (KKR) method,³³ where the full potential is represented by overlapping muffin-tin potential spheres. Inside these spheres, the potential is spherically symmetric and constant in between. By using overlapping spheres, one describes more accurately the exact crystal potential compared to conventional muffin-tin methods. Further details about the EMT0 method and its self-consistent implementation can be found in previous works.^{33–35,38,39} The accuracy of the EMT0 method for the equation of state, elastic properties, and the ideal strength in tension of metals and alloys has been demonstrated in a number of previous works.^{22,34,37,40–45}

The paramagnetic state of the Fe-based alloys was simulated by the so-called disordered local moment (DLM) model.⁴⁶ Within the DLM picture, the paramagnetic Fe and $\text{Fe}_{1-x}\text{M}_x$ binary alloys were described as a binary alloy $\text{Fe}\uparrow\text{Fe}\downarrow$ and a quaternary $(\text{Fe}\uparrow\text{Fe}\downarrow)_{1-x}(\text{M}\uparrow\text{M}\downarrow)_x$ alloy, with an equal amount of spin-up (\uparrow) and spin-down (\downarrow) components, respectively.

B. Ideal tensile strength calculations for bcc crystals

The principles of the response of bcc crystals to uniaxial loading were developed in a series of works by Milstein *et al.*^{47–49} In this work, we computed the ITS in the [001] direction of bcc Fe and Fe-based alloys. Since [001] was already identified to be the weakest direction of bcc Fe,^{18,19,21} here we concentrated on this direction only. Assuming an uniaxial tensile load, the tensile stress

$\sigma(\epsilon)$ can be calculated by¹⁵

$$\sigma(\epsilon) = \frac{1}{\Omega(\epsilon)} \frac{\partial E}{\partial \epsilon}, \quad (1)$$

where E is the total energy per atom and $\Omega(\epsilon)$ is the volume per atom at a given tensile strain, ϵ . The first maximum on the stress-strain curve defines the ITS, σ_m , for the selected deformation path with corresponding maximum strain, ϵ_m .

Uniaxial loading along the [001] direction reduces the symmetry of the bcc lattice to the body-centered tetragonal (bct) one on the primary deformation path. Clatterbuck *et al.*¹ reported a bifurcation from the primary deformation path to a secondary orthorhombic (orth) deformation path in Fe, however, the branching occurs for strains well above ϵ_m . Thus, an isotropic Poisson contraction along the Bain transformation path describes appropriately the symmetry of the distorted Fe lattice up to ϵ_m . The ideal tensile strength of the present Fe-alloys may nevertheless be influenced if this branching point shifts towards strains smaller than the maximum strain along the primary deformation path. We account for this possibility in this work.

On the primary tetragonal deformation path, the uniaxial strain energy,²² $\Delta E(c; [001])$, describes the total energy change upon deforming the bcc crystal in the [001] direction, and relaxing it with respect to the dimensions in the (001) plane,

$$\Delta E(c; [001]) = \min_a E(a, c) - E_0, \quad (2)$$

here a and c denote the lattice constants of the quadratic basal plane and the height of the bct unit cell, respectively. The initial undistorted state corresponds to the equilibrium bcc structure with energy E_0 and $c = a$. At $c/a = \sqrt{2}$, the bct lattice coincides with the face-centered cubic (fcc) lattice. On the secondary orthorhombic deformation path, we consider $\Delta E(a_{\text{orth}}, b_{\text{orth}}; [001])$ and minimize the total energy with respect to the lattice parameters of the face-centered orthorhombic lattice, a_{orth} and b_{orth} (to describe the bifurcation from the primary tetragonal to the secondary orthorhombic strain path, the face centered tetragonal reference frame of the Bain transformation is used²²).

For a more detailed technical description of ideal strength simulations with EMT0, we also refer the reader to Ref. 22

III. RESULTS

A. Ideal strength of bcc iron

To assess the reliability of our computational approach, we first performed the simulation of a tensile test in FM bcc Fe for uniaxial loading along the [001] direction. The theoretical equilibrium lattice parameter of bcc Fe

is 2.829 Å from our calculation, which agrees well with a full-potential value of, 2.830 Å.⁵⁰ The experimental lattice parameter, 2.868 Å,⁵¹ is 1.4% larger than the theoretical equilibrium value. The calculated spin magnetic moment of FM bcc Fe is 2.27 μ_B , which is approximately 2% larger than the measured value 2.22 μ_B .⁵² This overestimation of the magnetic moment of Fe is due to the employed GGA functional.

The magnetic order of the strained Fe lattice may change along the uniaxial loading process, which is for strains up to the branching point governed by the Bain transformation as discussed in the previous section. At zero strain, the ground state magnetic order is FM (bcc phase). The fcc state of Fe lying on the Bain transformation path (albeit at strains much larger than ϵ_m) exhibits a non-collinear spin arrangement as measured in fcc Fe precipitates and in thin fcc Fe films.^{53–55} That indicates that the ground state magnetic order of the strained bcc Fe lattice begins to differ from FM order at some particular strain in the range between bcc and fcc along the primary transformation path. If this would be the case for $\epsilon \leq \epsilon_m$, then additional magnetic order should be considered. However, there are strong indications that the FM order is the prevailing magnetic state for strains smaller than and somewhat above ϵ_m .^{20,56,57}

Clatterbuck *et al.*²⁰ computed the ideal strength of Fe in the [001] direction considering the FM order, a collinear anti-ferromagnetic structure (AFM, magnetic moment sequence $\uparrow\downarrow$) and a collinear double layer anti-ferromagnetic structure (DAFM, magnetic moment sequence $\uparrow\uparrow\downarrow\downarrow$). Their results show that Fe remains FM up to the point of its elastic instability during uniaxial tension, which lies at approximately $\epsilon_m = 15\%$ with $c/a \approx 1.16$ and $\Omega/\Omega_{\text{exp}} > 1$ (Ω_{exp} denotes the experimental atomic volume of bcc Fe). Further evidence is given by Tsetseris⁵⁶ and Friák *et al.*⁵⁷ which published minimum energy contour plots with respect to various magnetic orders (FM, AFM, and DAFM order by Friák *et al.* and non-collinear magnetism via a spin spiral formalism by Tsetseris) as a function of the bcc geometry thereby defining magnetic phase boundaries between different magnetic states. According to both references, FM order is the predominant magnetic order in the configuration space for $c/a \leq 1.25$ and $\Omega/\Omega_{\text{exp}} \geq 0.95$. Both references hence indicate that the point of elastic instability of Fe reported by Clatterbuck *et al.* is indeed located far from the borderline of FM order towards any other investigated magnetic ground state order. Hence, here we assume that Fe and also the present Fe-rich binary alloys stay FM during the deformation process.

The ideal tensile strength σ_m corresponding to the strain ϵ_m from our and other calculations in [001] direction for iron are listed in Table I. It can be seen that the three projector-augmented wave (PAW) works^{1,18,19} show similar stress values, however scatter somewhat in ϵ_m . Namely, Clatter *et al.*¹ reported a value of $\sigma_m = 12.6$ GPa at $\epsilon_m = 15\%$ and Liu *et al.*¹⁹ gave a value of $\sigma_m = 12.4$ GPa at $\epsilon_m = 14\%$. Furthermore, the two σ_m

TABLE I. The ideal tensile strength σ_m and the corresponding strain ϵ_m from our and published computations in [001] direction for a pure iron crystal. FP-LAPW stands for full-potential linearized augmented plane wave.

element	method	direction/[001]	
		σ_m (GPa)	ϵ_m (%)
Fe	EMTO	11.0	14
	PAW Ref. 1	12.6	15
	PAW Ref. 18	12.4	16
	PAW Ref. 19	12.4	14
	FP-LAPW Ref. 20	14.2	15
	FP-LAPW Ref. 21	12.7	15

values obtained by the all-electron full-potential linear augmented plane wave (FP-LAPW) method differ by 1.5 GPa ($\sim 11\%$). Compared to these theoretical full-potential data, the EMTO result for the stress of Fe is slightly smaller but still in reasonably good agreement. We obtained $c/a \approx 1.18$ and $\Omega/\Omega_{\text{exp}} \approx 1.04$ for the point of instability of Fe in agreement with Clatterbuck *et al.*²⁰ Finally, we computed that the bcc to ortho branching occurs at $\epsilon = 19\%$ well above ϵ_m in accordance with Ref. 1.

On the experimental side, the only attempt to measure the ideal tensile strength of Fe was by Brenner³ who tested Fe whiskers for tension was measured to be the [001] direction. The ITS of these Fe whiskers at room temperature was measured to be approximately 5 GPa. Compared to the theoretical data, the experimental value seems to be considerably lower. However, the observed failure initiated at the surface and, therefore, the measured value cannot be considered to represent bulk strength.

Based on the above results, we concluded that our theoretical tool is able to describe the ITS of bcc Fe with sufficiently high accuracy.

B. Ideal strength of Fe-based alloys

In the following we turn to bcc Fe-based alloys and investigate the effect of alloying elements $M = \text{Cr, Ni, Al, Co, Mn, and V}$ on the ITS of $\text{Fe}_{1-x}M_x$ random solid solutions. The selected solute atoms are common in commercial Fe-based steel alloys and they represent simple metal (Al), nonmagnetic (V) and magnetic (Cr, Co, Ni, and Mn) transition metals. The total concentration of these solutes was varied in the range from 0 to 10% except for Mn which the maximum concentration was 5%. The theoretical equilibrium lattice parameters of $\text{Fe}_{1-x}M_x$ ($M = \text{Cr, Ni, Al, Co, Mn and V}$) random alloys are displayed in Table II. We can see that compared to pure Fe, all alloying elements increase the lattice constant. Our computed lattice constants practically reproduce the earlier results from Ref. 28.

TABLE II. Theoretical (EMTO) lattice parameters $a(x)$ (in Å) calculated for the ferromagnetic bcc $\text{Fe}_{1-x}M_x$ alloys as a function of composition. For pure Fe, the value is $a(0) = 2.829$ Å.

x	$a(x)$					
	Fe-Cr	Fe-Co	Fe-V	Fe-Ni	Fe-Al	Fe-Mn
2.5	2.843	2.837	2.842	2.843	2.844	2.839
5	2.849	2.842	2.849	2.852	2.853	2.843
7.5	2.850	2.845	2.850	2.858	2.860	
10	2.849	2.848	2.858	2.861	2.866	

Figure 1 shows the composition dependence of the ITS of binary bcc Fe-based random alloys along the [001] direction and the corresponding numerical data for selected compositions are listed in Table II. The calculated ideal strength is found to increase with Cr, Co and V and decrease with Ni and Al addition to Fe. For instance, when 10% Cr, Co, or V is added to bcc Fe, the ITS of Fe increases by 1.4, 0.8 and 2.4 GPa, respectively. If however 10% Ni or Al are added to the Fe matrix, the ITS reduces by 1.5 GPa. For Mn, first the ITS increases weakly with increasing Mn amount below 2.5%, i.e., from 11.0 GPa to 11.3 GPa, then reduces by 0.3 GPa when up to 5% Mn is added to Fe compared to pure Fe. According to Fig. 1, it is clear that Al, Ni, and V show the strongest average alloying effect ($\Delta\sigma_m/\Delta x$) on the ITS of bcc Fe, whereas Mn, Ni and Cr produce intermediate alloying effect.

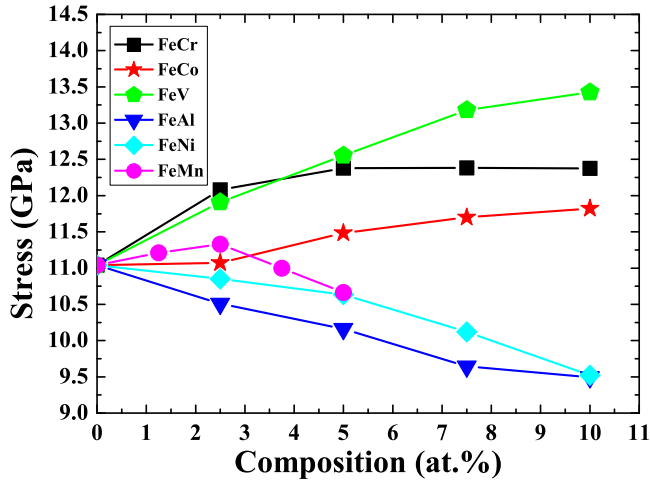


FIG. 1. (Color online) The ideal strength of Fe-based alloys as a function of composition.

We also considered the possibility of a branching from the primary bct deformation path to the secondary orthorhombic deformation path for the present Fe-based alloys. Based on these additional calculations, we can exclude a bifurcation from the primary bct deformation before the ideal strength is reached, i.e., for all alloys considered here the branching occurs at strains larger than ϵ_m .

IV. DISCUSSIONS

A. Failure of the structural energy difference model for ITS

Understanding the alloying effects on the ITS of Fe-based alloys is highly desirable. To this end, we start from a previously established simple model based in structural energy differences. For binary and ternary vanadium based $\text{V}_{1-y-z}\text{Cr}_y\text{Ti}_z$ random solid solutions, $0 \leq y + z \leq 0.1$, we established a qualitative correlation between the change of the ITS due to alloying and the change of the fcc-bcc structural energy difference (SED) of the alloy.²² Accordingly, the maximum stress (σ_m) was approximated by σ_m^{SED} along the [001] direction defined as

$$\sigma_m \approx \sigma_m^{\text{SED}} = \frac{1}{\Omega_{\text{bcc}}} \frac{\Delta E^{\text{SED}}}{\Delta \epsilon}, \quad (3)$$

where ΔE^{SED} denotes the SED at fixed volume (here of the bcc ground state, Ω_{bcc}) and $\Delta \epsilon$ is the strain at constant volume necessary to transform the bcc lattice into the fcc lattice along the Bain transformation ($\Delta \epsilon \approx 0.260$).

Equation. (3) is based on the fact that the fcc structure corresponds to the nearest maximum to the bcc phase of the uniaxial strain energy curve.^{1,19–21} Thus, the uniaxial strain energy must level off to the fcc-bcc energy difference, which implies a limitation on the maximum stress since it restricts $\Delta E(c; [001])$ to the SED within the strain interval to accomplish the transformation from bcc to fcc, i.e., the ratio $\Delta E^{\text{SED}}/\Delta \epsilon$ is bounded.

The alloying trend is captured by Eq. (3) if there is a correlation between the change of the ITS as a function of concentration, $\Delta\sigma_m(x)$, and the change of the fcc-bcc SED, $\Delta(\Delta E^{\text{SED}})(x)$. The prefactor $1/\Omega_{\text{bcc}}$ is weakly concentration dependent and does not change the conclusions drawn here. We show in the following that the correlation suggested by Eq. (3) fails for the bcc FM Fe-based alloys as opposed to the nonmagnetic $\text{V}_{1-y-z}\text{Cr}_y\text{Ti}_z$ alloys.²²

First, we assumed a FM state for both fcc Fe and the Fe-based alloys, since the FM fcc state of Fe was shown to be the nearest maximum of the uniaxial strain energy curve.^{1,19–21}

TABLE III. The ideal tensile strength σ_m , corresponding strain ϵ_m from our calculations in [001] direction for iron-based alloys.

composition	σ_m (GPa)	ϵ_m (%)	σ_m (GPa)	ϵ_m (%)	σ_m (GPa)	ϵ_m (%)
	Fe-Cr		Fe-Co		Fe-V	
2.5	12.1	14.0	11.1	14.2	11.9	14.8
5	12.4	14.7	11.5	15.2	12.6	15.3
7.5	12.4	14.5	11.7	14.9	13.2	15.3
10	12.4	14.2	11.8	15.1	13.4	15.3
	Fe-Ni		Fe-Al		Fe-Mn	
	σ_m (GPa)	ϵ_m (%)	σ_m (GPa)	ϵ_m (%)	σ_m (GPa)	ϵ_m (%)
2.5	10.9	14.3	10.5	14.7	11.3	14.6
5	10.6	14.3	10.2	14.6	10.7	14.4
7.5	10.1	13.6	9.7	14.4		
10	9.5	13.9	9.5	14.3		

Figure 2 displays $\Delta\sigma_m(x)$, obtained from the values in Table III, as a function of $\Delta(\Delta E^{\text{SED}})(x)$ calculated with EMTO-CPA. In figure, the alloying effect was obtained by increasing the concentration of the solute from 0 % to 5 %. We can see that Ni, Mn, and Al decrease the ITS and also decrease the SED, however, Co, Cr, and V increase the ITS but decrease the SED. We also investigated the correlation between σ_m and ΔE^{SED} increasing the concentration of the solute from 5 % to 10 %, however the result is qualitatively identical to the one depicted in Fig. 2. From these results, we infer that the anticipated correlation between the ITS and the FM SEDs following Eq. (3) can not capture the observed alloying trend of σ_m .

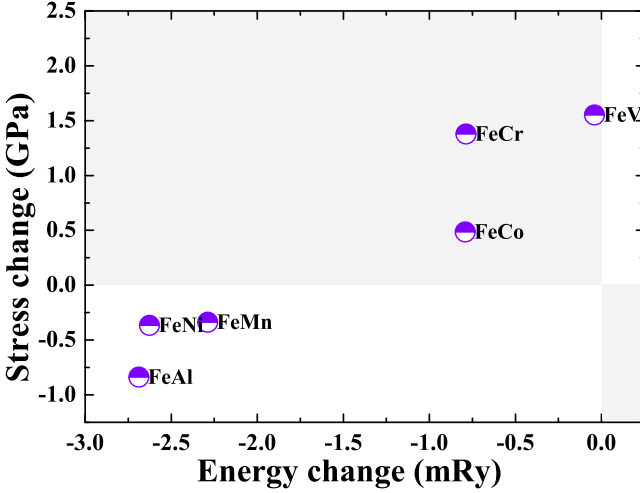


FIG. 2. (Color online) The change of the ITS, $\Delta\sigma_m$ versus the change of the fcc-bcc SED, $\Delta(\Delta E^{\text{SED}})$, for $\text{Fe}_{1-x}\text{M}_x$ alloys assuming a FM fcc state for a concentration increase of the solute from 0 % to 5 %. Data in unshaded areas affirm a correlation based on Eq. (3).

Next we tried to establish a correlation between the PM SEDs obtained from paramagnetic (PM) fcc $\text{Fe}_{1-x}\text{M}_x$ alloys and their FM bcc phases. Using the

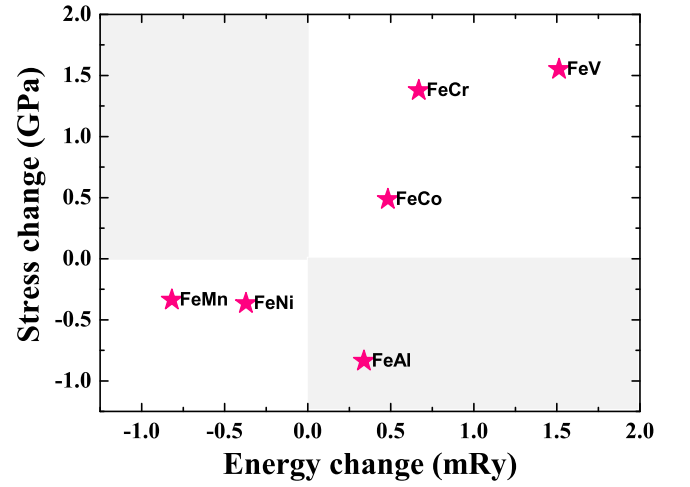


FIG. 3. (Color online) The change of the ITS, $\Delta\sigma_m$ versus the change of the fcc-bcc SED, $\Delta(\Delta E^{\text{SED}})$, for $\text{Fe}_{1-x}\text{M}_x$ alloys assuming a paramagnetic fcc state for a concentration increase of the solute from 0 % to 5 %. Data in unshaded areas affirm a correlation based on Eq. (3).

above described procedure and a concentration increase of the solute from 0 % to 5 %, we plotted the stress change versus the PM SED change in Fig. 3. From that figure, it can be clearly seen that Ni and Mn decrease the ITS and likewise decrease the SED, while Cr, Co, and V increase the ITS as well as they increase the PM SED. However, FeAl is outlying as the ITS decreases with Al, but the PM SED increases with Al. Assuming a paramagnetic fcc state thus captures somewhat better the observed alloying trends than a FM fcc but the correlation dictated by Eq. (3) is still not perfect.

One possible reason why Eq. (3) is not a good estimate for the alloying trend of σ_m for Fe alloys may be related to the different employed deformations paths. Along the unconstrained primary deformation path of tensile stress, the volume of the unit cell can change and a is determined from Eq. (2). Fcc-bcc SEDs on the other hand

were computed at the bcc equilibrium volume, i.e., on a Bain deformation path at constant volume Ω_{bcc} , where a is given by $2\Omega_{\text{bcc}}/c^2$. Equation (3) captures the alloying trend on σ_m , if the effect of alloying on the total energy is comparable for both strain paths. That was indeed the case for nonmagnetic V-based random alloys.²² However, for the present FM Fe-based alloys the interplay between magnetism and the structure in Fe along the deformations paths should also be considered. We provide arguments in the following section, that the above failure can indeed be originated in the effect of magnetism.

B. Magnetic effects on the ITS

To achieve a better understanding of the matter, we computed an auxiliary ideal stress assuming a constant volume deformation, i.e., the maximum stress according to Eq. (1) was deduced from the total energy computed as a function of strain for fixed unit cell volume. The constant volume for each Fe-alloy is the one of its theoretical equilibrium volume (Table II). The so-calculated maximum stress at constant volume, σ_m^Ω , with maximum strain, ϵ_m^Ω , is then correlated to FM ΔE^{SED} from Eq. (3). Since both values were obtained for the same strain path, we expect that the correlation between σ_m^Ω and ΔE^{SED} significantly improves for all alloys, despite possible interference from magnetism.

First, σ_m^Ω as an approximate to the ideal strength of Fe-based alloys as a function of the alloying elements is displayed in Fig. 4. Notice the difference between Fig. 1 and Fig. 4, the prior corresponding to relaxed volume and the latter to constrained volume. According to Fig. 4, the constrained ITS decreases with increasing composition for all alloying elements compared to the value of Fe. Al, Ni, and Mn solutes have a stronger effect than the other elements.

Compared to the ideal stresses depicted in Fig. 1 (with variable volume), the constrained-ITSs keep their trends as a function of x in the case of Al, Ni, and Mn, but the ITS shows an opposite trend for Cr, Co, and V addition. Figure 5 displays the correlation between the change of the constrained-ITS calculated at the constant volume, $\Delta\sigma_m^\Omega(x)$, and the change of the FM SED ($\Delta(\Delta E^{\text{SED}})(x)$). Both alloying effects for an increase of the concentration of the solute from 0% to 5% and for an increase from 5% to 10% are displayed. Quite interestingly, we obtain that the change in the constrained-ITS correlates well with the SED change.

By comparing Fig. 4 with Fig. 1, it is immediately evident that the ideal strength of Fe is most significantly affected by the fixed volume constraint, i.e., it increases from 11.0 GPa to 16.0 GPa. This is unlike the Fe-alloys with moderate solute concentrations, where the ideal strength increases are considerably smaller the higher the solute concentration are, e.g., we obtained an increase from 13.4 GPa to 15.1 GPa for Fe-10V.

An answer to the observed correlation may be given

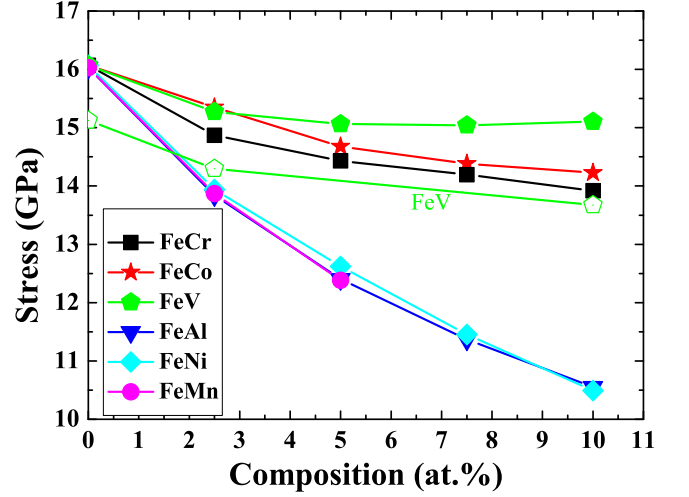


FIG. 4. (Color online) The ideal strength σ_m^Ω of Fe-based alloys as a function of composition at a constant volume deformation (closed symbols). The open pentagons are the ideal strengths of FeV alloys with fix magnetic moment along the relaxed volume deformation.

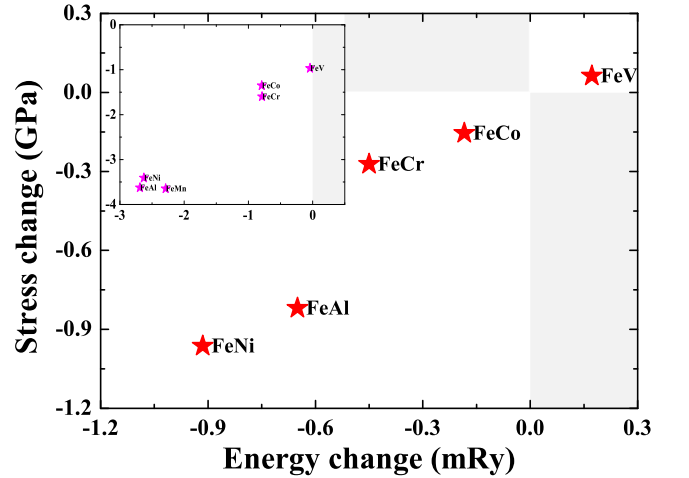


FIG. 5. (Color online) The change of the ITS for constant volume, $\Delta\sigma_m^\Omega$ versus the change of the fcc-bcc SED, $\Delta(\Delta E^{\text{SED}})$, for $\text{Fe}_{1-x}M_x$ alloys assuming a FM fcc state for a concentration increase of the solute from 5% to 10% and from 0% to 5% (inset). Data in unshaded areas affirm a correlation between $\Delta\sigma_m^\Omega$ and ΔE^{SED} .

by considering magnetism in Fe and its alloys. In the following we chose Fe-10V as a representative of all investigated binary alloys. The total energy and the spin magnetic moment of Fe are opposed to those of Fe-10V in Fig. 6, where we plotted both quantities as a function of the tetragonal axial ratio (c/a) and the Wigner-Seitz radius, ω . We also displayed the corresponding uniaxial deformation path in the range from $\epsilon = 0 \dots \epsilon_m$.

As visible from the contour plots, the magnetic mo-

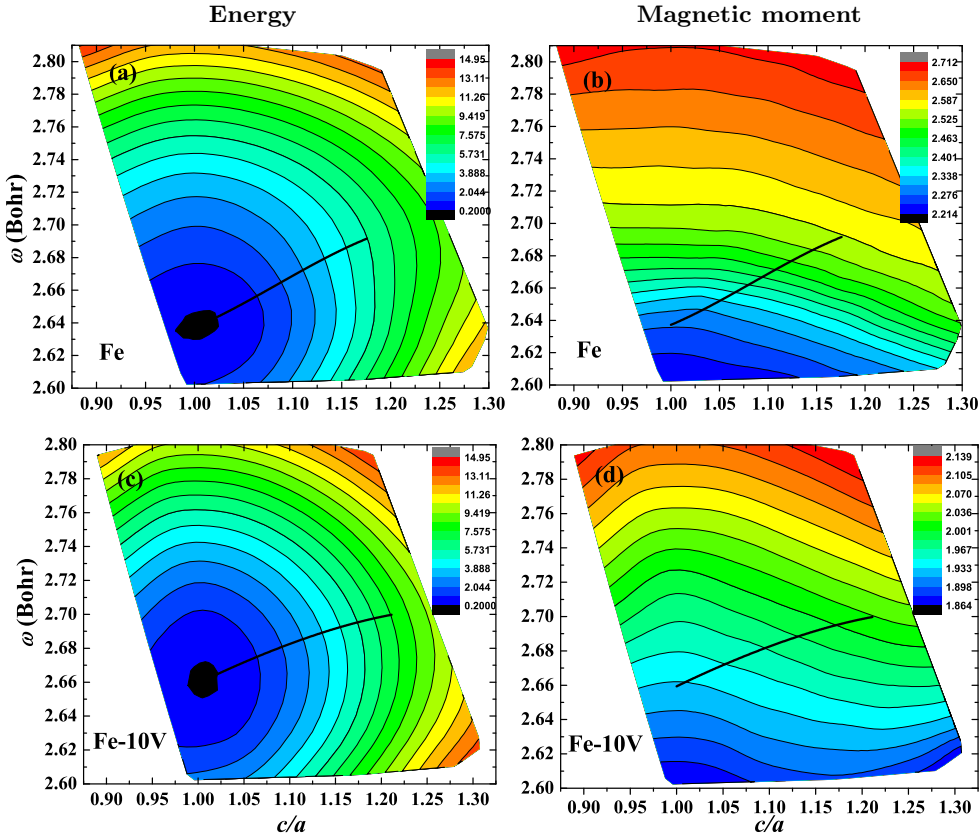


FIG. 6. (Color online) Total energy (in mRy) and magnetic moments (in μ_B) contours for pure Fe (upper panel) and V-10V alloy (lower panel) as a function of the tetragonal ratio (c/a) and Wigner-Seitz radius (ω in bohrs). The energy are plotted relative to the bcc ($c/a = 1$) minimum. Figures (a) and (c) are total energy contours, (b) and (d) are magnetic moments contours. The black solid lines show the uniaxial deformation paths in the range from $\epsilon = 0 \dots \epsilon_m$.

ment increase of Fe along the deformation allowing for a volume change from $\epsilon = 0 \dots \epsilon_m$ is much stronger than the one of Fe-10V; the numbers read $0.27 \mu_B$ and $0.09 \mu_B$ for Fe and the Fe-10V alloy, respectively. These numbers are in contrast to the deformation at constant volume (in the range $\epsilon = 0 \dots \epsilon_m^\Omega$), where the changes are $0.09 \mu_B$ for Fe and $0.03 \mu_B$ for Fe-10V. That indicates that the increase of the atomic volume has a more pronounced influence on the relaxation of the magnetic moment than the structural change (c/a), a result which can be clearly associated with the contour lines in Fig. 6. It should be noted that $|\epsilon_m^\Omega - \epsilon_m|$ is at most 1.5% (for one and the same material), i.e., ϵ_m^Ω is quite similar to ϵ_m for Fe and the present Fe-alloys.

Now, alloying Fe with any of the solutes under investigation in this work increases the equilibrium volume (Table II). Unconstrained uniaxial tensile loading is also accompanied by an increase of the volume per atom, as depicted in Fig. 7 for Fe and for the Fe-based alloys with the highest considered solute concentrations. In the region of the maximum strains, both Fe and the Fe alloys have rather similar volumes as opposed to the situation at equilibrium. The volume change of Fe due to the

deformation is thus distinctly larger than those of the Fe-based alloys. According to our numerical data (also Fig. 6), the larger volume increase of Fe is paralleled by a larger magnetic moment increase along the uniaxial deformation from equilibrium to ϵ_m , despite the fact that Fe contributes only by a factor of $1 - x$ to the magnetic moment of the alloys.

The comparatively large increase of the magnetic moment in Fe along the uniaxial deformation path with unconstrained volume and the pronounced difference between σ_m^Ω and σ_m (5 GPa) may, at least in parts, be related. We recall, that both the increase of the magnetic moment and the difference $\sigma_m^\Omega - \sigma_m$ of all Fe-alloys are smaller than the values of Fe. To substantiate this correlation, we recalculated the ITSs for the previously determined unconstrained strain paths but with fixed magnetic moments, i.e., the magnetic moments were not allowed to relax to self-consistency. We employed the respective ground state magnetic moments of Fe and the Fe-V alloys.

Fixing the magnetic moment increases the resulting computed strengths, but the increase is strongly diminished with higher solute concentration, e.g., approxi-

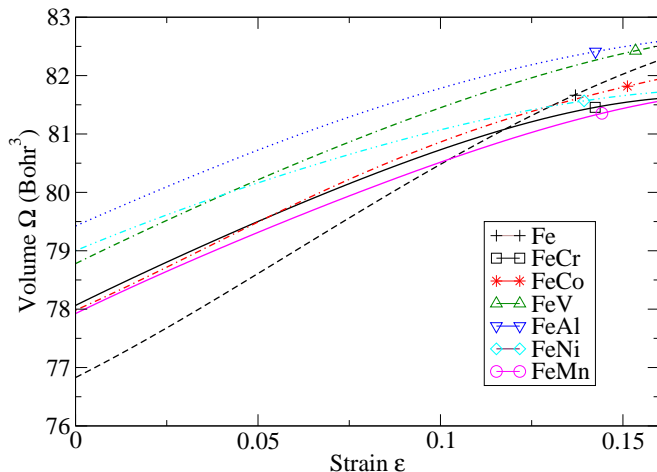


FIG. 7. (Color online) The volume per atom of Fe and of Fe-based alloys with 10 % solute concentration (5 % solute concentration in the case of Mn) as a function of strain for the unconstrained deformation path. The open symbols specify the volumes at the maximum strain.

mately 4.0 GPa for Fe but only 0.2 GPa for Fe-10V. The previous numbers may be obtained by comparing σ_m from Fig. 1 with the ITSs obtained with the fixed-spin moment constraint depicted in Fig. 4 (open pentagons). The latter strength values are plotted in comparison to the previously determined ITSs computed without a constraint on the magnetic moments but for fixed volume (σ_m^Ω). The alloying trend that both curves for Fe-V follow in Fig. 4 is alike, and the resulting stresses are essentially much larger than σ_m of Fe (4.0 GPa for the fixed-spin moment value and 5.0 GPa for σ_m^Ω) but only slightly to moderately larger than σ_m of Fe-10V (0.2 GPa for the fixed-spin moment value and 1.6 GPa for σ_m^Ω). Thus, fixing the volume but allowing for a relaxation of the magnetic moments produces essentially the same alloying effect than fixing the magnetic moment but taking into account structural relaxations.

However, as we pointed out above, the magnetic moment is almost unchanged along the constant volume deformation owing to the weak influence of the c/a ratio. Thus, we conclude, that the main contribution to the difference of σ_m^Ω and σ_m originates from a magnetic contribution to the total energies which is associated with the relaxation of the spin magnetic moment to its self-consistent value. This magnetic contribution is accordingly the largest for Fe, which can be partly ascribed to the comparatively small volume at equilibrium. Both the reduced volume change and the involved reduced magnetic contribution to the stress bring forth the convergence of σ_m^Ω to σ_m for the investigated Fe-alloys with 10 % solute concentration.

Returning in conclusion to Eq. (3), the correlation between σ_m and σ_m^{SED} fails due to magnetism in Fe and the investigated Fe alloys. That is, the alloying trend on the fcc-bcc SEDs at fixed volume can not capture the

alloying trend on the energy-strain landscape and hence the ITS of the uniaxial deformation path as opposed to nonmagnetic V-Ti-Cr alloys.²²

V. CONCLUSIONS

The ideal tensile strengths of bcc ferromagnetic Fe and $\text{Fe}_{1-x}M_x$ ($M=\text{Cr, Ni, Al, Co, Mn, and V}$) random alloys in the [001] direction have been investigated using the all-electron exact muffin-tin orbitals method in combination with the coherent-potential approximation. The present calculated ideal strength value of Fe and the branching point from the primary bcc deformation path to the secondary orthorhombic deformation path of Fe agree well with previously published results, which thus confirms that our methodology has the accuracy needed for such kind of calculations. For the Fe-based alloys, we found that the ideal strength increases with increasing concentration of Cr, Co, and V and decreases with Ni and Al addition into pure Fe. Mn shows a non-monotonous alloying behavior. Unlike the nonmagnetic bcc V-based alloys investigated in our previous paper,²² constant volume fcc-bcc structural energy differences can not entirely capture the alloying effect on the ideal tensile strength for the FM bcc Fe-based alloys. By calculating auxiliary ideal strengths assuming a constant volume deformation (σ_m^Ω) and fixed-spin moment calculations along the (kept unaltered) tetragonal deformation paths, we showed that mainly the interplay between the volume increase and magnetic moment increase along the tetragonal deformation paths lead to a failure of the correlation between σ_m and σ_m^{SED} .

The present results offer a consistent starting point for further theoretical modeling of the micro-mechanical properties of Fe-based alloys. Based on these achievements, we conclude that the EMTO-CPA approach provides an efficient and accurate theoretical tool to design the mechanical strength of ferromagnetic bcc random solid solutions. Nevertheless, in such applications one should always monitor the basic muffin-tin and single-site CPA errors and make sure that they remain at acceptable level as a function of the lattice distortion and chemical composition.

VI. ACKNOWLEDGEMENTS

The Swedish Research Council, the Swedish Steel Producers' Association, the European Research Council, the China Scholarship Council and the Hungarian Scientific Research Fund (research project OTKA 84078), and the National Magnetic Confinement Fusion Program of China (2011GB108007) are acknowledged for financial support. S. S. gratefully acknowledges the Carl Tryggers Stiftelse för Vetenskaplig Forskning and Olle Erikssons stiftelse för materialteknik.

-
- * xiaoqli@kth.se
† stes@kth.se
‡ zhaojj@dlut.edu.cn
- ¹ D. M. Clatterbuck, D. C. Chrzan, and J. W. Morris, Jr., *Acta Mater.* **51**, 2271 (2003).
 - ² A. Kelly and N. H. Macmillan, *Strong Solids* (Clarendon, Oxford, 1986).
 - ³ S. S. Brenner, *J. Appl. Phys.* **27**, 1484 (1956).
 - ⁴ M. Yoshida, T. Sumomogi, T. Endo, H. Maeta, and T. Kino, *Mater. Trans.* **48**, 1 (2007).
 - ⁵ Y. J. Wang and C. Y. Wang, *Appl. Phys. Lett.* **94**, 261909 (2009).
 - ⁶ M. Šob, L. G. Wang, and V. Vitek, *Mater. Sci. Eng., A* **234-236**, 1075 (1997).
 - ⁷ W. Li and T. Wang, *Phys. Rev. B* **59**, 3993 (1999).
 - ⁸ Y. Umeno and T. Kitamura, *Mater. Sci. Eng. B* **88**, 79 (2002).
 - ⁹ K. Yashiro, M. Oho, and Y. Tomita, *Comp. Mater. Sci.* **49**, 397 (2004).
 - ¹⁰ H. B. Zhou, Y. Zhang, Y. L. Liu, M. Kohyama, P. G. Yin, and G. H. Lu, *J. Phys.: Condens. Matter* **21**, 175407 (2009).
 - ¹¹ A. T. Paxton, P. Gumbsch, and M. Methfessel, *Phil. Mag. Lett.* **63**, 267 (1991).
 - ¹² N. Nagasako, M. Jahnátek, R. Asahi, and J. Hafner, *Phys. Rev. B* **81**, 094108 (2010).
 - ¹³ D. Roundy, C. R. Krenn, M. L. Cohen, and J. W. Morris, Jr., *Phys. Rev. Lett.* **82**, 2713 (1999).
 - ¹⁴ W. D. Luo, D. Roundy, M. L. Cohen, and J. W. Morris, Jr., *Phys. Rev. B* **66**, 094110 (2002).
 - ¹⁵ D. Roundy, C. R. Krenn, M. L. Cohen, and J. W. Morris, Jr., *Philos. Mag. A* **81**, 1725 (2001).
 - ¹⁶ C. R. Krenn, D. Roundy, J. W. Morris, Jr., and M. L. Cohen, *Mater. Sci. Eng. A* **319-321**, 111 (2001).
 - ¹⁷ M. Černý and J. Pokluda, *Phys. Rev. B* **82**, 174106 (2010).
 - ¹⁸ M. Černý and J. Pokluda, *Phys. Rev. B* **76**, 024115 (2007).
 - ¹⁹ Y. L. Liu, Y. Zhang, R. J. Hong, and G. H. Lu, *Chin. Phys. B* **18**, 1923 (2009).
 - ²⁰ D. M. Clatterbuck, D. C. Chrzan, and J. W. Morris, Jr., *Phil. Mag. Lett.* **82**, 141 (2002).
 - ²¹ M. Šob, M. Friák, D. Legut, J. Fiala, and V. Vitek, *Mat. Sci. Eng. A* **387-389**, 148 (2004).
 - ²² X. Q. Li, S. Schönecker, J. J. Zhao, B. Johansson, and L. Vitos, under review (2013).
 - ²³ R. Klueh, D. Gelles, S. Jitsukawa, A. Kimura, G. Odette, B. van der Schaaf, and M. Victoria, *J. Nucl. Mater.* **307**, 455 (2002).
 - ²⁴ A. Kohyama, Y. Kohno, K. Satoh, and N. Igata, *J. Nucl. Mater.* **122**, 619 (1984).
 - ²⁵ G. R. Spaich, A. J. Schwoeble, and W. C. Leslie, *Metall. Trans.* **3**, 2031 (1972).
 - ²⁶ G. R. Spaich and W. C. Leslie, *Metall. Trans.* **4**, 1873 (1973).
 - ²⁷ S. Takeuchi, *J. Phys. Soc. Jpn* **27**, 929 (1969).
 - ²⁸ H. L. Zhang, M. P. J. Punkkinen, B. Johansson, S. Hertzmann, and L. Vitos, *Phys. Rev. B* **81**, 184105 (2010).
 - ²⁹ V. I. Razumovskiy, A. V. Ruban, and P. A. Korzhavyi, *Phys. Rev. B* **84**, 024106 (2011).
 - ³⁰ X. Q. Li, J. J. Zhao, and J. C. Xu, *Front. Phys.* **7**, 360 (2012).
 - ³¹ P. Hohenberg and W. Kohn, *Phys. Rev. B* **136**, 864 (1964).
 - ³² J. P. Perdew, K. Burke, and M. Ernzerhof, *Phys. Rev. Lett.* **77**, 3865 (1996).
 - ³³ O. K. Andersen, O. Jepsen, and G. Krier, in *Lectures on Methods of Electronic Structure Calculations*, edited by V. Kumar, O. K. Andersen, and A. Mookerjee (World Scientific, Singapore, 1994) p. 63.
 - ³⁴ L. Vitos, *Phys. Rev. B* **64**, 014107 (2001).
 - ³⁵ L. Vitos, H. L. Skriver, B. Johansson, and J. Kollár, *Comput. Mater. Sci.* **18**, 24 (2000).
 - ³⁶ B. L. Gyorffy, *Phys. Rev. B* **5**, 2382 (1972).
 - ³⁷ A. Taga, L. Vitos, B. Johansson, and G. Grimvall, *Phys. Rev. B* **71**, 014201 (2005).
 - ³⁸ L. Vitos, I. A. Abrikosov, and B. Johansson, *Phys. Rev. Lett.* **87**, 156401 (2001).
 - ³⁹ L. Vitos, *Computational Quantum Mechanics for Materials Engineers* (Springer-Verlag, London, 2007).
 - ⁴⁰ L. Huang, L. Vitos, S. K. Kwon, B. Johansson, and R. Ahuja, *Phys. Rev. B* **73**, 104203 (2006).
 - ⁴¹ J. Zander, R. Sandström, and L. Vitos, *Comput. Mater. Sci.* **41**, 86 (2007).
 - ⁴² B. Magyari-Köpe, G. Grimvall, and L. Vitos, *Phys. Rev. B* **66**, 064210 (2002).
 - ⁴³ B. Magyari-Köpe, L. Vitos, and G. Grimvall, *Phys. Rev. B* **70**, 052102 (2004).
 - ⁴⁴ L. Vitos, P. A. Korzhavyi, and B. Johansson, *Nat. Mater.* **2**, 25 (2003).
 - ⁴⁵ X. Q. Li, H. L. Zhang, S. Lu, W. Li, J. J. Zhao, B. Johansson, and L. Vitos, *Phys. Rev. B* **86**, 014105 (2012).
 - ⁴⁶ B. L. Gyorffy, A. J. Pindor, J. Staunton, G. M. Stocks, and H. Winter, *J. Phys. F: Met. Phys.* **15**, 1337 (1985).
 - ⁴⁷ F. Milstein, *Phys. Rev. B* **2**, 512 (1970).
 - ⁴⁸ F. Milstein, *Phys. Rev. B* **3**, 1130 (1971).
 - ⁴⁹ F. Milstein and J. Marschall, *Phil. Mag. A* **58**, 365 (1988).
 - ⁵⁰ F. Tran, R. Laskowski, P. Blaha, and K. Schwarz, *Phys. Rev. B* **75**, 115131 (2007).
 - ⁵¹ V. N. Staroverov, G. E. Scuseria, J. Tao, and J. P. Perdew, *Phys. Rev. B* **69**, 075102 (2004).
 - ⁵² C. Kittel, *Introduction to Solid State Physics*, Vol. 23 (Wiley, New York, 1986).
 - ⁵³ Y. Tsunoda, *J. Phys.: Condens. Matter* **1**, 10427 (1989).
 - ⁵⁴ Y. Tsunoda, H. Nogami, and M. Takasaka, *Phys. Rev. B* **76**, 054419 (2007).
 - ⁵⁵ H. L. Meyerheim, J.-M. Tonnerre, L. Sandratskii, H. C. N. Tolentino, M. Przybylski, Y. Gabi, F. Yildiz, X. L. Fu, E. Bontempi, S. Grenier, and J. Kirschner, *Phys. Rev. Lett.* **103**, 267202 (2009).
 - ⁵⁶ L. Tsetseris, *Phys. Rev. B* **72**, 012411 (2005).
 - ⁵⁷ M. Friák, M. Šob, and V. Vitek, *Phys. Rev. B* **63**, 052405 (2001).